Effect of Boundary-Layer Transition on Vehicle Dynamics

LARS ERIC ERICSSON*
Lockheed Missiles & Space Company, Sunnyvale, Calif.

The effect of boundary-layer transition on vehicle dynamics is a well known, but poorly understood, phenomenon. Severe loss of dynamic stability has been observed to result on ablating vehicles when boundary-layer transition moves up over the base onto the aft body. This effect is caused by the increased (turbulent) aft body heating, and is equivalent to changing to a coating with higher ablation rate on the aft body. Another more subtle effect of boundary-layer transition results from the transition sensitivity to body attitude. Dynamic tests of nonablating slender cones have shown that increased damping and decreased static stability results when boundary-layer transition occurs on the aft body. An analysis using previously developed unsteady concepts for separated flow correctly predicts the relation between dynamic and static effects of boundary-layer transition. The dynamic amplification of static effects is twice as large for sharp as for blunted cones because of oscillatory flow acceleration effects on the sharp cone boundary-layer transition. It is found that the boundary-layer transition sensitivity to body attitude has beneficial effects on the vehicle dynamics up to high supersonic speeds. However, at hypersonic speeds nose-bluntness-induced entropy swallowing may cancel and even reverse this trend, greatly aggravating the undamping effect of turbulent aft body (heating and) ablation.

Nomenclature

C_m = $M_p/(\rho_\infty U_\infty{}^2/2)Sc$
C_{m_q} = $\partial C_m/\partial(cq/U_\infty)$
C_N = $N/(\rho_\infty U_\infty{}^2/2)S$
C_{N_α} = $\partial C_N/\partial\alpha$
c = reference length, m
d = local body diameter, m
k = proportionality constant, Eq. (12)
l = body length, m
l_o = sharp cone body length, m
M_p = pitching moment, kgm
M = Mach number
N = normal force, kg
p = static pressure, kg/m^2
q = rigid body pitch rate, rad/sec
R_l = Reynolds number based on body length
S = $\pi c^2/4$ = reference area, m^2
t = time, sec
Δt = time lag, sec
U = velocity, m/sec
x = axial body fixed coordinate, m
α = angle of attack, rad or deg; $\dot{\alpha} = \partial\alpha/\partial t$
α_o = trim angle of attack, rad or deg
$\Delta\alpha$ = oscillatory amplitude, rad or deg
γ = ratio of specific heats
Δ = difference or increment
δ = boundary-layer thickness, m
δ^* = boundary-layer displacement thickness, m
θ = body attitude perturbation, rad or deg
ν = Prandtl-Meyer angle, rad or deg
ξ = dimensionless axial coordinate, $\xi = x/c$ (Fig. 7)
ρ = air density, kg-sec^2/m^4
ω = rigid body pitching frequency, rad/sec

Subscripts

B,N = base and nose, respectively
e = edge of boundary layer
tr = boundary-layer transition
1,2 = forebody and aftbody lumped load stations, respectively, (Fig. 7)
∞ = freestream conditions

Superscripts

i = induced, $\Delta^i C_{N_{tr}}$ = change in (aft) body normal force due to boundary-layer transition as affected by upstream (forebody) crossflow
— = barred quantities denote mean values

Presented as Paper 69-106 at the AIAA 7th Aerospace Sciences Meeting, New York, January 20–27, 1969; submitted January 30, 1969; revision received August 11, 1969. J. P. Reding, Lockheed Missiles & Space Company, has contributed decisively to the development of the (separated) flow concepts on which this paper is based. Because of other commitments, J. P. Reding could not participate in the writing of the present paper to the degree he considers commensurate with coauthorship.

*Senior Staff Engineer. Associate Fellow AIAA.

Introduction

WHEN boundary-layer transition moves up over the base of a slender re-entry body, the effects on vehicle dynamics can be dramatic. On an ablating vehicle, severe loss of dynamic stability may result.[1] However, on nonablating vehicles, the boundary-layer transition has a beneficial effect on the dynamic stability, as has been shown by Ward[2] (Fig. 1). Recent data obtained at Arnold Engineering Development Center on a more slender blunted cone confirms Ward's results and shows even greater effects of boundary-layer transition (Fig. 2). An analysis is presented that predicts the observed relation between dynamic and static effects of boundary-layer transition. At angle of attack the boundary-layer build-up on the leeward side generates a negative aft body force, causing a slight decrease of static stability and a somewhat larger increase of dynamic stability. When the boundary layer is either purely laminar or turbulent, the effects of boundary-layer build-up are small. This is at least true for a nonablating vehicle below hypersonic speeds. However, when transition occurs, the boundary-layer build-up effects become appreciable even on a nonablating vehicle. On a sharp cone the time-lagged boundary-layer build-up effects are augmented by flow acceleration effects, further delaying the boundary-layer transition.

Discussion

The compressible laminar and turbulent boundary-layer growth on a sharp cone at $\alpha = 0$ can be computed using Mangler-transformed flat plate values.[3,4] Neglecting the effect of boundary-layer displacement thickness on the "effective body geometry" could possibly lead to overesti-

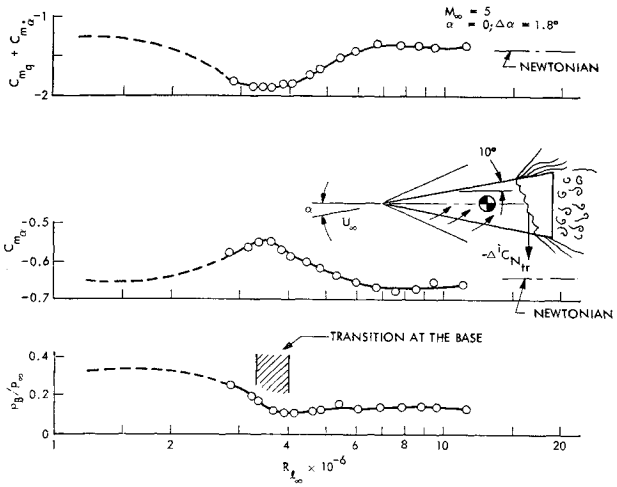

Fig. 1 Boundary-layer transition effects on sharp cone stability.[2]

mation of aerodynamic coefficients by up to 15% in low-density hypersonic flow (Fig. 3). More important, however, is the marked difference in boundary-layer growth rates between turbulent and laminar flows. The corresponding difference ($\Delta\nu$) in displacement surface slope between top and bottom surfaces in the region of transition (using the transition line concept) can be appreciable. The resulting differential pressure coefficient ΔC_p is not large in itself (Fig. 4), but when it is combined with the tremendous sensitivity of transition to angle of attack[2] (Fig. 5), respectable normal force derivatives are obtained (Fig. 6). The observed change in static stability (ΔC_{m_α}), extracted from the experimental data as shown in Fig. 2, is well predicted by this normal force derivative ΔC_{N_α} (Fig. 6).

Quasi-Steady Analysis

The dynamic effects of boundary-layer transition are derived using the quasi-steady methodology developed in Ref. 1. Forces C_{N_1} and C_{N_2} in Fig. 7 are of attached flow

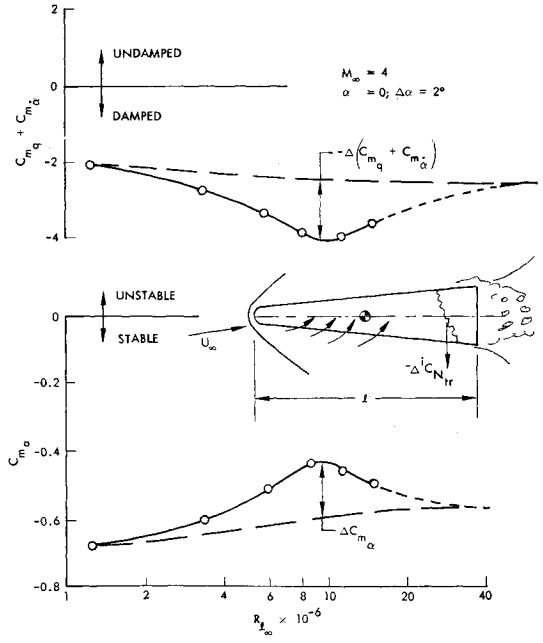

Fig. 2 Boundary-layer transition effects on blunted cone stability.

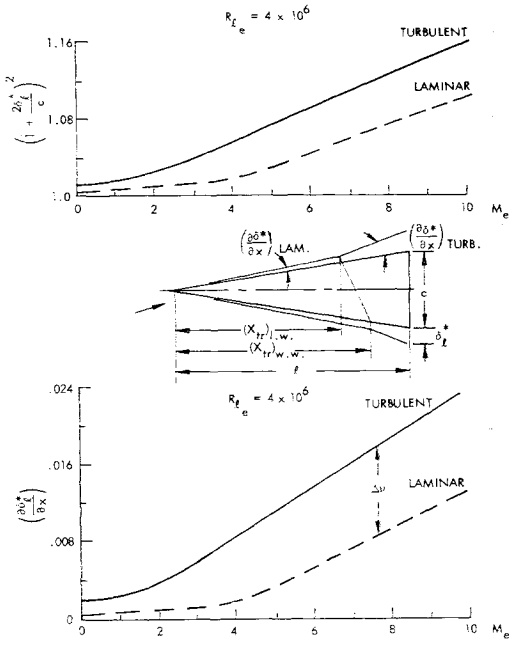

Fig. 3 Compressible boundary-layer growth on a sharp cone.

type (inviscid), whereas $\Delta^i C_{N_{tr}}$ is the negative (aft) body force induced by differential (top and bottom) boundary-layer transition. The earlier transition on the leeward side is the result of the forebody crossflow thickening and weakening the leeward side boundary layer. Using the lumped force representation of Ref. 1, the quasi-steady boundary-layer thickness can be expressed as follows:

$$\delta(x_{tr},t) = (\delta)_{\substack{\alpha=0\\ \dot\alpha=0}} + (\partial\delta/\partial\alpha)_1\,\tilde\alpha\,(x_1,t-\Delta t_1) + (\partial\delta/\partial\alpha)_2\tilde\alpha(x_2 t-\Delta t_2) \quad (1)$$

$\tilde\alpha$ is the angular representation of body crossflow; Δt_1 and Δt_2 are the time increments occurring before changes of body crossflow at x_1 and x_2, respectively, have resulted in changed boundary-layer thickness at transition (x_{tr}). For rigid body oscillations around the center of gravity (Fig. 7) $\tilde\alpha$ is simply

$$\tilde\alpha = \alpha_o + \theta + \xi c\dot\theta/U_\infty \quad (2)$$

For slow oscillations at the low reduced frequencies realizable for re-entry bodies, $(c\omega/U_\infty)^2 \ll 1$, $\alpha(t-\Delta t)$ can be expressed as follows:

$$\alpha(t-\Delta t) = \alpha(t) - \Delta t\dot\alpha(t) \quad (3)$$

$$\Delta t = (\bar x_{tr} - x)/\bar U = (\bar\xi_{tr} - \xi)(U/U_\infty)^{-1}c/U_\infty \quad (4)$$

$\bar U$ is boundary-layer convection speed, $0.8 \le \bar U/U_\infty \le 1.0$.

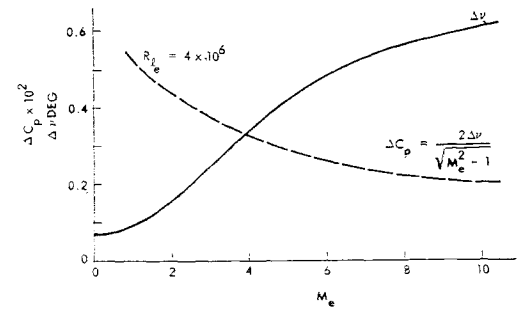

Fig. 4 Transition-induced boundary-layer shape change and associated pressure increase on a pointed slender cone.

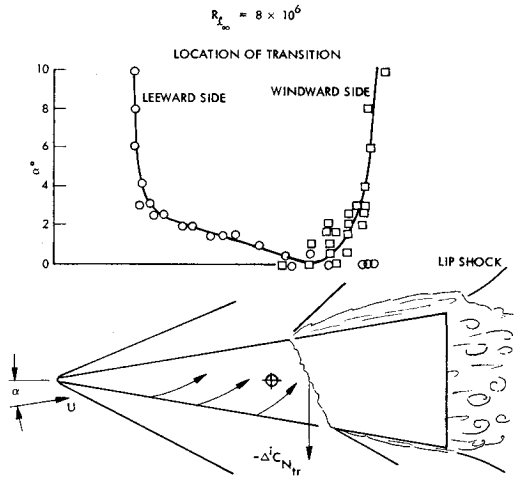

Fig. 5 Effect of angle of attack on boundary-layer transition on a 10° sharp cone.[2]

Thus, the induced force $\Delta^i C_{N_{tr}}$ can be written as follows, lumping the induced forces at $\bar{x}_{tr}$:

$$\Delta^i C_{N_{tr}} = \Delta^i C_{N_{tr}}(\alpha_o) + \frac{\partial \Delta^i C_{N_{tr}}}{\partial \delta}\left(\frac{\partial \delta}{\partial \alpha}\right)_1 \times \left\{\theta + \left[\xi_1 - \frac{(\bar{\xi}_{tr} - \xi_1)}{\bar{U}/U_\infty}\right]\frac{c\dot{\theta}}{U_\infty}\right\} + \frac{\partial \Delta^i C_{N_{tr}}}{\partial \delta}\left(\frac{\partial \delta}{\partial \alpha}\right)_2 \times \left\{\theta + \left[\xi_2 - \frac{(\bar{\xi}_{tr} - \xi_2)}{\bar{U}/U_\infty}\right]\frac{c\dot{\theta}}{U_\infty}\right\} \quad (5)$$

If the effect of the near aft body crossflow at x_2 is neglected (the effect should be small at near zero angle of attack), Eq. (5) gives

$$\partial \Delta^i C_{N_{tr}}/\partial\theta = (\partial \Delta^i C_{N_{tr}}/\partial\delta)(\partial\delta/\partial\alpha)_1 = \Delta^i C_{N_{\alpha_{tr}}}$$

$$\frac{\partial \Delta^i C_{N_{tr}}}{\partial(c\dot{\theta}/\bar{U}_\infty)} = \Delta^i C_{N_{\alpha_{tr}}}\left[\xi_1 - \frac{(\bar{\xi}_{tr} - \xi_1)}{\bar{U}/U_\infty}\right] = C_{N_\alpha} \quad (6)$$

With $C_m = -\bar{\xi}_{tr} C_N$, Eq. (6) gives the boundary-layer build-up effect shown in Fig. 8. It can be seen that the boundary-layer build-up does not account for the observed dynamic effect of transition. The dynamic amplification of the static boundary-layer transition effect is given by Eq. (6), and is

$$\frac{\Delta(C_{m_q} + C_{m_{\dot\alpha}})}{\Delta C_{m_\alpha}} = \frac{\Delta C_{N_{\dot\alpha}}}{\Delta C_{N_\alpha}} = \xi_1 - \frac{(\bar{\xi}_{tr} - \xi_1)}{\bar{U}/U_\infty} \quad (7)$$

Figure 9 shows that the boundary-layer build-up effect accounts for all the dynamic amplifications observed on the blunted cone, but only for part of the amplification observed on the sharp cone. In the latter case, the remainder is due to accelerated flow effects. The boundary-layer transition is affected by accelerated flow much the same way as flow

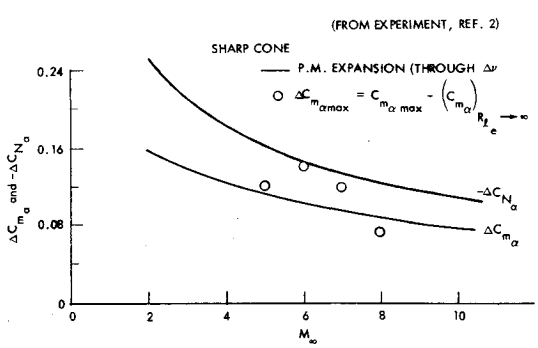

Fig. 6 Computed and measured aerodynamic effects on boundary-layer transition.

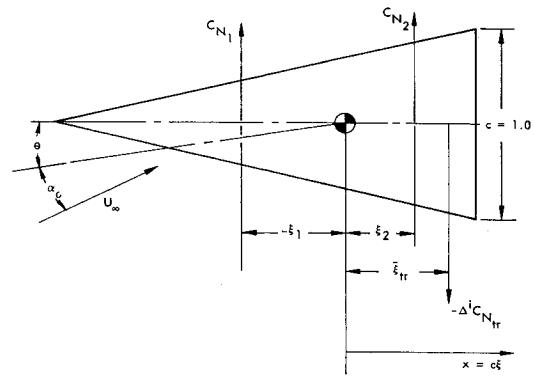

Fig. 7 Definitions for lumped force analysis.

separation is.[5,6] That is, the location x_{tr} of boundary-layer transition is not only determined by the boundary-layer build-up, but is also dependent upon the local pressure gradient and Mach number (as affected by the oscillatory perturbations). On the blunted slender cone the favorable pressure gradient generated by the nose bluntness is substantial, and the changes due to angle-of-attack perturbations are minor in comparison. Consequently, the dynamic amplification on the blunt cone is almost entirely accounted for by boundary-layer build-up. That the amplification still is much larger on the blunted cone is due to its shallow surface slope. The blunt cone half-angle is only 60% of the sharp cone value. How powerful the nose bluntness effect is in delaying separation is illustrated by the data in Fig. 10. A slightly less blunt cone has appreciably earlier transition, as the lesser nose bluntness causes less delay of the boundary-layer transition.

On the sharp cone, however, with zero pressure gradient at $\alpha = 0$, attitude perturbations around $\alpha = 0$ will have large effects on the pressure gradient, and will delay the boundary-layer transition by the same mechanism that delays shock-induced flow separation on cone-cylinder bodies.[5,6]

The pressure gradient of the external flow at the edge of the boundary layer is given by the complete Bernoulli equation

$$-(1/\rho_e)dp_e/dx = \partial U_e/\partial t + U_e \partial V_e/\partial x \quad (8)$$

or, with $\xi = x/c$,

$$dp_e/d\xi = -\rho_e U_e[(\partial U_e/\partial t)(c/U_e) + \partial U_e/\partial \xi] \quad (9)$$

For constant vehicle velocity, U_e changes only through body

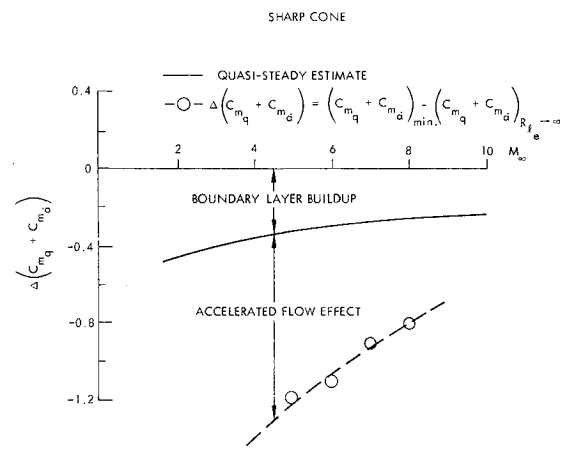

Fig. 8 Comparison between predicted and measured effects of boundary-layer transition on sharp cone dynamic stability.

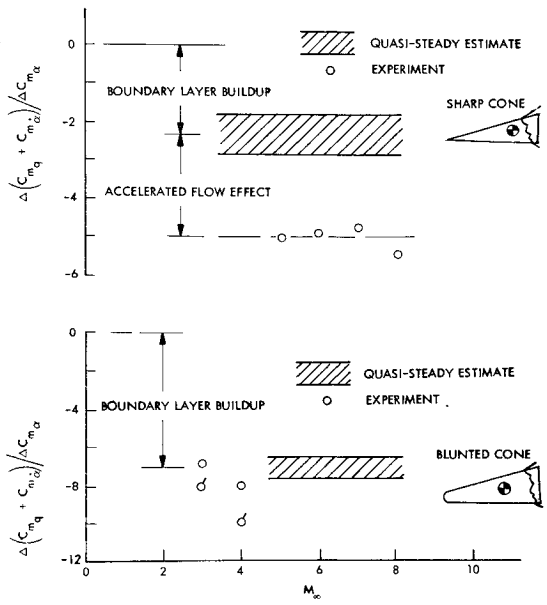

Fig. 9 Comparison between predicted and measured dynamic amplification of transition-induced static stability changes on sharp and blunted cones.

pitching; thus,

$$dp_e/d\xi = -\rho_e U_e[(\partial U_e/\partial\alpha)(c\dot{\alpha}/U_e) + \partial U_e/\partial\xi] \quad (10)$$

That is

$$dp_e/d\xi = (dp_e/d\xi)_{\dot{\alpha}=0} + (\partial p_e/\partial\alpha)(c\dot{\alpha}/U_e) \quad (11)$$

$\partial p_e/\partial\alpha$ can be expressed by a Prandtl-Meyer expansion through an "effective expansion angle" proportional to ν. That is,

$$\partial p_e/\partial\alpha = k\partial p_e/\partial\nu \approx -kp_e\gamma M_e^2(M_e^2 - 1)^{-1/2} \quad (12)$$

Equations (11) and (12) show that body pitching, $(c\dot{\alpha}/U_e) > 0$, will decrease the pressure gradient and will, therefore, delay boundary-layer transition. That is, the transition will in the unsteady case lag behind its static or steady-state position. This lag, added to the lag in the boundary-layer build-up, makes the dynamic amplification of the sharp cone in Fig. 9 more than twice as large as it would have been due to boundary-layer build-up alone.

Comparing the stability levels at high and low Reynolds numbers, that is, on both sides of the large boundary-layer

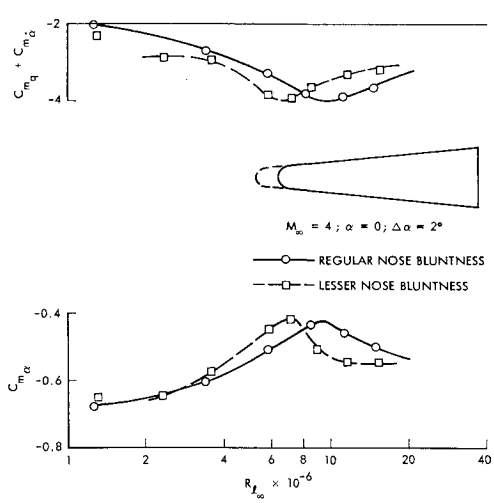

Fig. 10 Effect of nose bluntness on boundary-layer transition on a slender cone.

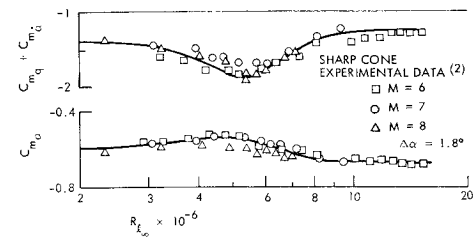

Fig. 11 Effect of Reynolds number on sharp cone stability at hypersonic speeds.[2]

transition effects, it appears that the low Reynolds number data show a loss of static stability and a gain of dynamic stability relative to the high Reynolds number data. This is at least true for the pointed cone (Fig. 11), and is to be expected for the following reasons. Assuming that the high Reynolds-number turbulent boundary-layer data show inviscid stability levels, the decreased static and increased dynamic stability at low Reynolds numbers would be caused by laminar boundary-layer build-up effects. The same type of dynamic amplification effect as for the boundary-layer transition could be expected, although the magnitude would be somewhat lower. $\bar{\xi}_{tr}$ in Eq. (7) has to be replaced by ξ_2 (Fig. 7) when lumping the leeward side boundary-layer build-up (and windward side boundary-layer thinning). Figure 11 seems to agree with this observation, indicating levels of $\Delta(C_{m_q} + C_{m_{\dot{\alpha}}})/\Delta C_{m_\alpha}$ between -1 and -2, compared to -2 to -3 for the transition effect (Fig. 9). Thus, sharp cone data are nice and orderly, corroborating the presented unsteady flow hypothesis.

The blunted cone data, however, do not corroborate this turbulent-laminar correlation. The trends are exactly the opposite (compare Figs. 2 and 11). In order to resolve this unfortunate anomaly, one has to scrutinize the experimental setup. Figure 12 shows the measured variation of static and dynamic stability with angle of attack. The flow was laminar for all the Mach numbers tested; still only Mach numbers 5 and 5.9 showed the expected (attached flow) angle-of-attack trends. Going back to the test setup, one finds that the sting used in combination with a concave base could cause the deviations shown at smaller angles of attack for $M = 3$ and $M = 4$, when transition occurs in the near wake. The reason that the $M = 5$ and $M = 5.9$ data do not

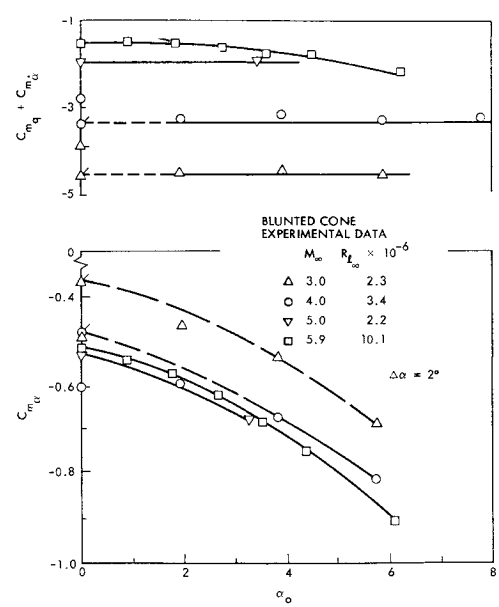

Fig. 12 Effect of angle of attack on blunted cone stability characteristics.

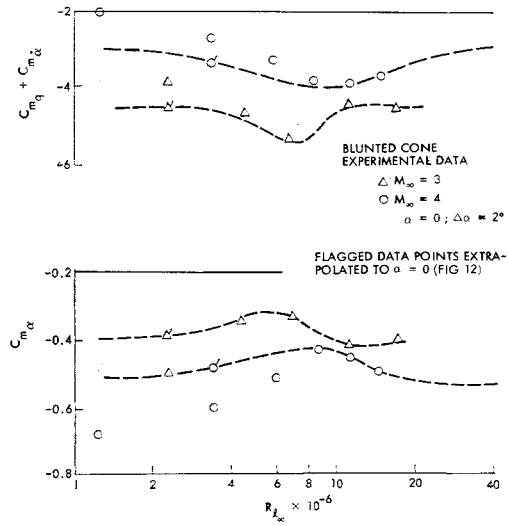

Fig. 13 Effect of Reynolds number on blunted cone stability after correction for sting interference.

show the interference is probably that in the former case transition occurred well downstream of the near wake (R_{l_∞} = 2.2 × 10⁶), whereas for M = 5.9 transition occurred on the cone (R_{l_∞} = 10.1 × 10⁶). As the sting interference is concentrated to low angles of attack,[7] one can extrapolate the high angle-of-attack data down to α = 0 for M = 3 and M = 4, following the attached flow trends exhibited by the data for M = 5 and M = 5.9. The thereby obtained "correct" flagged data points for α = 0 are shown in Fig. 13, together with the measured ("uncorrected") data. Using the extrapolated data fairing in Fig. 13 to extract stability increments due to boundary-layer transition gives the flagged data points in Fig. 9. It can then be concluded that on the blunted cone the influence of oscillatory flow acceleration on the dynamic effects of boundary-layer transition are small and often can be neglected. It is likewise indicated (Fig. 13) that the laminar boundary-layer build-up effects on blunted cone dynamics is negligibly small, again probably due to the favorable pressure gradient induced by the nose bluntness.

In light of what has just been said about sting interference effects on the blunted cone, it is pertinent to reexamine the sharp cone data for possible sting interference. If the data in Figs. 1 and 11 were affected by sting interference, the effects would be largest for the low Reynolds number data

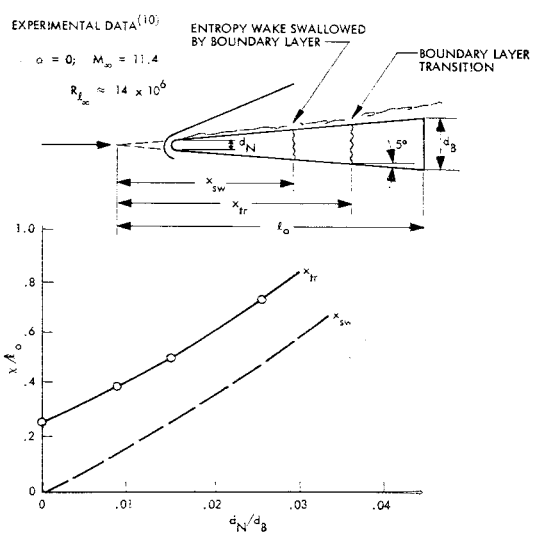

Fig. 14 Effect of entropy swallowing on boundary-layer transition on a slender cone.[10]

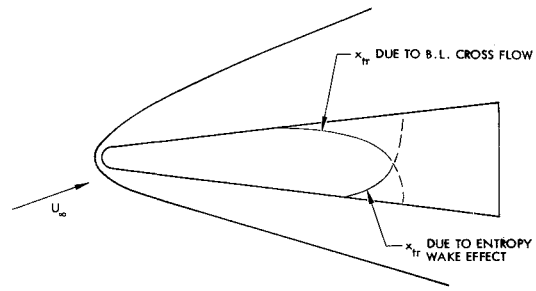

Fig. 15 Composite effects of boundary-layer cross flow and entropy swallowing on the boundary-layer transition on slender cones.

obtained with a laminar boundary layer over the cone. If the sting interference were of the cylindrical variety,[7] the "corrected" laminar data would show increased dynamic and decreased static stability levels.† This would bring the dynamic amplification factor (Eq. 7) with ξ_2 substituted for $\bar{\xi}_{tr}$, to unrealistic levels above those obtained for the boundary-layer transition effect. In view of this and the fact that the turbulent (inviscid) sharp cone data agrees well with theoretical predictions by the method of characteristics,[8] one can conclude that the sharp cone measurements were free of sting interference effects.

At hypersonic speeds other complications enter into the unsteady aerodynamics of a blunted cone. The nose bluntness induced bow shock curvature creates a downstream nonuniform flowfield, an "entropy wake." Even in inviscid flow the nose bluntness can severely degrade the dynamic stability.[9,10] The high flow shear created downstream will control the boundary-layer transition, as has been shown by Softley et al.[11] (Fig. 14). Correspondingly, the earlier entropy swallowing on the windward side may at hypersonic speeds cause boundary-layer transition to occur earlier on the windward than on the leeward side, as has been observed by Cleary.[12,13] This entropy swallowing effect, combined with the leeward side boundary-layer thickening effect, could lead to the peculiar boundary-layer transition geometry sketched in Fig. 15. This competition with the leeward side transition movement will prevent the entropy swallowing from aggravating the dynamically destabilizing effects of aft body ablation to the extent previously assumed.[14]

When the base of the cone is not flat but round-shouldered or dome-shaped, the hypersonic unsteady aerodynamics are further complicated. The addition of a bulbous base degrades the dynamic stability of a slender reentry vehicle.[15] When boundary-layer transition occurs near the base, it has a very strong influence on the bulbous base effect, with nose bluntness again being capable of reversing the effects of this coupling between boundary-layer transition and the flow over the bulbous base.[16]

Conclusions

A quasi-steady analysis which lumps the effects of time history to one discrete past event has predicted experimentally observed effects of boundary-layer transition on the stability characteristics of (nonablating) slender cones. The following conclusions can be drawn.

Due to the sensitivity of boundary-layer transition to body attitude, it will appreciably affect vehicle stability when it starts occurring on the aft body. It will decrease the static stability somewhat but increase the dynamic stability much more, relatively speaking, order of magnitudes larger if the body is very slender. This dynamic

† Any interference of the flared sting or hollow base variety would bring the laminar stability data to the unnatural levels existing for the blunted cone before the correction for sting interference.

amplification decreases if the cone is blunted. At hypersonic speeds the nose-bluntness-induced entropy swallowing effects may cancel or even reverse the beneficial effect of boundary-layer transition on nonablating vehicle dynamics.

On ablating cones, the effects of boundary-layer sensitivity to body attitude will have an alleviating influence on the adverse dynamic effects associated with the increased aft body ablation when transition moves up on the body.

References

[1] Ericsson, L. E. and Reding, J. P., "Ablation Effects on Vehicle Dynamics," *Journal of Spacecraft and Rockets*, Vol. 3, No. 10, Oct. 1966, pp. 1476–1483.

[2] Ward, L. K., "Influence of Boundary-Layer Transition on Dynamic Stability at Hypersonic Speeds," *Transactions of the Second Technical Workshop on Dynamic Stability Testing*, Paper 9, Vol. II, April 1965, Arnold Engineering Development Center, Arnold Air Force Station, Tenn.

[3] Schlichting, H., *Boundary Layer Theory*, 4th ed., McGraw-Hill, New York, 1960.

[4] Eckstrom, D. J., "Engineering Analysis of Boundary Layers and Skin Friction on Bodies of Revolution at Zero Angle of Attack," TM 55-21-21, LMSC/805162, May 1965, Lockheed Missiles & Space Co.

[5] Ericsson, L. E., "Aeroelastic Instability Caused by Slender Payloads," *Journal of Spacecraft and Rockets*, Vol. 4, No. 1, Jan. 1967, pp. 65–73.

[6] Ericsson, L. E., "Steady and Unsteady Terminal Shock Aerodynamics on Cone-Cylinder Bodies," LMSC L-87-67-2, Contract NAS 8-20354, Oct. 1967, Lockheed Missiles & Space Co., Sunnyvale, Calif.

[7] Reding, J. P. and Ericsson, L. E., "Dynamic Support Interference on Bulbous Based Configurations," 3rd Technical Workshop on Dynamic Stability Problems, NASA Ames Research Center, Nov. 4–7, 1968.

[8] Rie, H., Linkiewicz, E. A., and Bosworth, F. D., "Hypersonic Dynamic Stability, Part III, Unsteady Flow Field Program," FDL-TDR-64-149, Pt. III, Jan. 1967, Air Force Flight Dynamics Lab., Wright-Patterson Air Force Base.

[9] Ericsson, L. E., "Unsteady Aerodynamics of an Ablating Flared Body of Revolution Including Effect of Entropy Gradient," *AIAA Journal*, Vol. 6, No. 12, Dec. 1968, pp. 2395–2401.

[10] Ericsson, L. E. and Scholnick, I. M., "Effect of Nose Bluntness on the Hypersonic Unsteady Aerodynamics of Flared and Conical Bodies of Revolution," AIAA Paper 68-889, Pasadena, Calif., 1968; also *Journol of Spacecraft and Rockets*, Vol. 6, No. 3, March 1969, pp. 321–324.

[11] Softley, E. J., Graber, B. C., and Zempel, R. E., "Experimental Observation of the Hypersonic Boundary Layer," AIAA, Paper 68-39, New York, 1968; also *AIAA Journal*, Vol. 7, No. 2, Feb. 1969, pp. 257–263.

[12] Cleary, J. W., "Effects of Angle of Attack and Nose Bluntness on the Hypersonic Flow Over Cones," AIAA Paper 66-414, Los Angeles, Calif., 1966.

[13] Cleary, J. W., "An Experimental and Theoretical Investigation of the Pressure Distribution and Flow Fields of Blunted Cones at Hypersonic Mach Numbers," TND-2969, Aug. 1965, NASA.

[14] Ericsson, L. E., "Effect of Nose Bluntness on the Hypersonic Unsteady Aerodynamics of an Ablating Re-entry Body," *Journal of Spacecraft and Rockets*, Vol. 4, No. 6, June 1967, pp. 811–813.

[15] Ericsson, L. E. and Reding, J. P., "Effect of Bulbous Bases on Reentry Vehicle Dynamics," 3rd Technical Workshop on Dynamic Stability Problems, NASA Ames Research Center, Nov. 4–7, 1968.

[16] Ericsson, L. E. and Reding, J. P., "Aerodynamic Effects of Bulbous Bases," LMSC 4-17-68, Contract NAS 1-6450, Nov. 1968, Lockheed Missiles & Space Co., Sunnyvale, Calif.; also CR-1339, Aug. 1969, NASA.